Zuse Institute Berlin

Takustr. 7
14195 Berlin
Germany

SOURAV RAY, ARNE THIES, VIKRAM SUNKARA, M. ÖZGÜR CELIK, FATIH YERGÖZ, CHRISTOF SCHÜTTE, CHRISTOPH STEIN, MARCUS WEBER, STEFANIE WINKELMANN

Modelling altered signalling of G-protein coupled receptors in inflamed environment to advance drug design

ZIB Report 21-19 (July 2021)

Zuse Institute Berlin
Takustr. 7
14195 Berlin
Germany

Telephone: +49 30 84185-0
Telefax: +49 30 84185-125

E-mail: bibliothek@zib.de
URL: http://www.zib.de

ZIB-Report (Print) ISSN 1438-0064
ZIB-Report (Internet) ISSN 2192-7782

Modelling altered signalling of G-protein coupled receptors in inflamed environment to advance drug design

Sourav Ray[1,†], **Arne Thies**[2,†], **Vikram Sunkara**[1,2], **M. Özgür Celik**[3], **Fatih Yergöz**[3], **Christof Schütte**[1,2], **Christoph Stein**[3], **Marcus Weber**[1,‡], **Stefanie Winkelmann**[1,‡]

***For correspondence:**
weber@zib.de (MW);
winkelmann@zib.de (SW)

[†]These authors contributed equally to this work
[‡]These authors also contributed equally to this work

Present address: [§]Departments of Modelling and Simulation of Complex Processes, Zuse Institute Berlin, 14195 Berlin, Germany

[1]Zuse Institute Berlin, 14195 Berlin, Germany; [2]Freie Universität Berlin, Institut für Mathematik und Informatik, 14195 Berlin, Germany; [3]Institute of Experimental Anaesthesiology, Charité Universitätsmedizin Berlin, 12200 Berlin, Germany

Abstract Initiated by mathematical modelling of extracellular interactions between G-protein coupled receptors (GPCRs) and ligands in normal versus diseased (inflamed) environments, we previously reported the successful design, synthesis and testing of the prototype opioid painkiller NFEPP that does not elicit adverse side effects. Uniquely, this design recognised that GPCRs function differently under pathological versus healthy conditions. We now present a novel stochastic model of GPCR function that includes intracellular dissociation of G-protein subunits and modulation of plasma membrane calcium channels associated with parameters of inflamed tissue (pH, radicals). By means of molecular dynamics simulations, we also assessed qualitative changes of the reaction rates due to additional disulfide bridges inside the GPCR binding pocket and used these rates for stochastic simulations of the corresponding reaction jump process. The modelling results were validated with *in vitro* experiments measuring calcium currents and G-protein activation. We found markedly reduced G-protein dissociation and calcium channel inhibition induced by NFEPP at normal pH, and enhanced constitutive G-protein activation but lower probability of ligand binding with increasing radical concentrations. These results suggest that, compared to radicals, low pH is a more important determinant of overall GPCR function in an inflamed environment. Future drug design efforts should take this into account.

Introduction

The family of G-protein coupled receptors (GPCRs) represents the largest class of receptors in the human genome and some of the most common drug targets. Located on the cell membrane, they transduce extracellular signals into key physiological effects. Natural GPCR ligands include neurotransmitters, chemokines, hormones, odours or photons. GPCRs are involved in a large number of disorders, such as diabetes, high blood pressure, depression, addiction, pain, arthritis, Parkinson's and many others (***Congreve et al., 2020***). A prominent member of this family is the μ-opioid receptor (MOR). Recent works of our group (***Spahn et al., 2017***) led to the development of the novel analgesic compound N-(3-fluoro-1-phenethylpiperidin-4-yl)-N-phenylpropionamide (NFEPP) which activates the MOR preferentially at acidic extracellular pH-levels, as given in injured tissues (***Stein, 2018***). This is of utmost interest because it may preclude the adverse effects of conventional MOR agonists like fentanyl which include constipation, sedation and apnea. These adverse effects

are mediated mostly in the brain and the gut, i.e. in healthy tissues (pH 7.4). Since the generation of pain can be effectively inhibited at the site of the injury (i.e. the origin of nociceptive stimulation), this gives rise to the hope that NFEPP might have less or even no adverse effects, which could already be corroborated in animal studies (***Spahn et al., 2017***; ***Rodriguez-Gaztelumendi et al., 2018***; ***Massaly et al., 2020***; ***Jimenez-Vargas et al., 2021***).

Up to now, the effects of NFEPP and fentanyl were mathematically analysed at the level of their binding rates at relevant amino acid residues accessible from the extracellular side of MOR (***Spahn et al., 2017***; ***Ray et al., 2020***). To get a more complete picture, we have here built a model of the intracellular second messenger pathways relevant to pain and analgesia. The mechanism underlying the analgesic effect of MOR activation in nociceptive neurons is mainly due to a stabilisation or even lowering of the plasma membrane potential beneath the threshold value required to elicit an action potential (reviewed in ***Stein*** (***2018***); ***Bhave and Gereau*** (***2004***)). This effect is mediated via intracellular inhibitory G-proteins, which dissociate into α- and $\beta\gamma$-subunits after formation of a receptor-ligand complex (***Weis and Kobilka, 2018***). Among other actions, the $\beta\gamma$-subunits bind to calcium channels in the plasma membrane. This leads to closure of the channels, thereby lowering the amount of positive calcium-ion influx and reducing cellular excitability (reviewed in ***Proft and Weiss*** (***2015***); ***Zamponi et al.*** (***2015***); ***Stein*** (***2018***); ***Bhave and Gereau*** (***2004***)). In this paper, we modelled this pathway with a stochastic approach to analyse the effects of fentanyl and NFEPP on the number of closed membrane calcium channels and activated (i.e. dissociated) G-protein complexes at different pH-levels. We constructed a biochemical reaction network that connects the receptor-ligand interactions to the G-protein cycle, and further to the signal cycle of calcium channel opening and closing (see Fig. 1 for an illustration). The corresponding stochastic reaction process was simulated for different values of the receptor-ligand binding rate, comparing the mean inhibition of calcium currents and the mean activation of G-proteins resulting from these numerical simulations to corresponding data from *in vitro* experiments. It is important to note that our approach differs from others that have investigated signalling pathways from receptor to the nucleus or to intracellular second messengers (not to the plasma membrane) by using deterministic instead of stochastic models (***Shaw et al., 2019***; ***Bridge et al., 2018***). As the duration of membrane calcium channel inhibition required for an efficient reduction of pain signals varies widely (depending on the nature of noxious stimulation), we chose a stochastic model rather than ordinary differential equations.

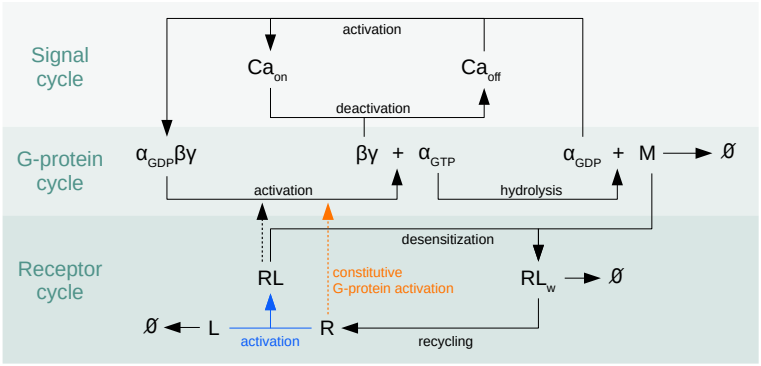

Figure 1. Overview of the reaction network. Biochemical reaction network for the μ-opioid receptor signalling pathway, connecting the receptor cycle to the G-protein cycle and further to the signal cycle of membrane calcium channel activation. The basic reaction network was extended by the constitutive G-protein activation (orange). The focal point of this study is the analysis of the impact that the rates for ligand-induced receptor activation (blue) and for constitutive G-protein activation (orange) have onto the overall dynamics.

Aside from pH, other inflammatory mediators play important roles. For example, reactive oxygen species (radicals) can induce disulfide bond (DSB) formation in opioid receptors (***Bowen and Pert, 1982***). In *in vitro* experiments, reactive oxygen species can be added by using hydrogen per-

oxide (H_2O_2). In order to understand the interplay between pH and additional DSB inside MOR for the signalling, we modelled different scenarios (see Fig. 2) and performed molecular dynamics (MD) simulations. Whereas pH has a major influence on the binding rate of opioids to MOR (see Tab. 1), conformational changes based on DSB can alter the position of transmembrane helix 6 (TM6) of MOR without any opioid bound. This showed that DSB inside the binding pocket might initiate constitutive G-protein activation with a certain probability. This led us to an extension of the above model, adding the reaction of constitutive G-protein dissociation. By this extension, it is possible to take into account conformational changes of the MOR due to DSB. In summary, two different influences and three different effects are analysed in this article:

1) A lower pH value changes the protonation state of amino acid residues and opioid ligands, and thus changes their binding rates and subsequent modulation of calcium channels (first effect).
2) An increased concentration of radicals leads to DSB formation, which reduces the binding affinity of ligands (second effect) and increases the probability for constitutive G-protein dissociation (third effect).

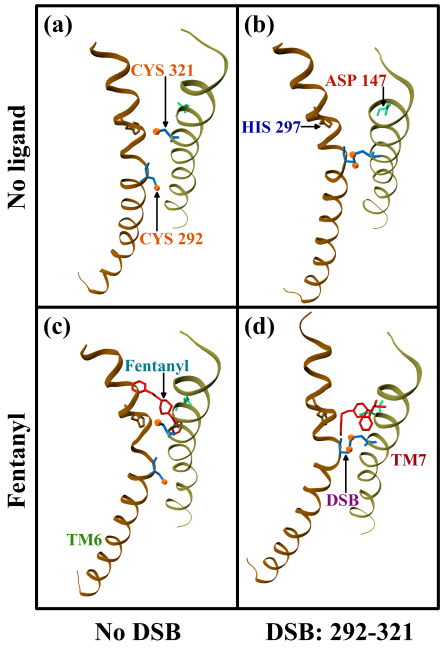

Figure 2. Simulation setup. Trajectory snapshot at 5 ns of μ-opioid receptor (MOR) without (a, b) and with (c, d) the ligand fentanyl, and without (a, c) and with (b, d) an additional CYS $292^{6.47}$ – CYS $321^{7.38}$ DSB (for terminology, see (***Isberg et al., 2015***)). The figures show the two neighbouring helices TM6 and TM7 of the MOR. Interaction between the ligand and the MOR is assessed by measuring the distance between the ligand, and the two amino acid residues ASP $147^{3.32}$ and HIS $297^{6.52}$.

Results

In this section, we present the results of our studies on the two influences of pH value and additional DSB and the three different effects regarding the signalling dynamics.

Impact of the pH value

We first considered the basic biochemical reaction network, which is illustrated in Fig. 1 (omitting the constitutive G-protein activation) and described in more detail in Materials and Methods. Our goal was to analyse the effect of varying rates $k_1 > 0$ for the ligand-induced activation of a receptor (given by the binding reaction $\mathcal{R}_1 : L + R \to RL$, see Tab. 2 in Materials and Methods) onto the

amount of closed calcium channels Ca_{Off}. We examined the ligands fentanyl and NFEPP in combination with changing pH levels (see Tab. 1 for the respective rate values). The relative change of k_1 was deduced from ***Ray et al.*** (***2020***). The rates for the other reactions were left unchanged in all simulations based on the assumption that the intracellular situation does not change much with different extracellular levels of pH and/or radicals.

Fig. 3a represents the mean number of closed calcium channels depending on time for the different ligand-binding rates k_1 given in Tab. 1. Note that for the pairings fentanyl (pH 5.5), NFEPP (pH 5.5) and NFEPP (pH 6.5), the same binding rate k_1 was used. For $k_1 \in \{2.5\times10^{-2}s^{-1}, 1.25\times10^{-2}s^{-1}\}$ we observed similar amplitudes of closed calcium channels (about 46% of all calcium channels), while $k_1 = 2.5\times10^{-3}s^{-1}$ slightly reduced the amplitude and $k_1 = 5\times10^{-4}s^{-1}$ significantly decreased the amplitude to approximately 29% (but note that only a maximum of 40 out of the total of 80 channels can be closed since there are only 40 G-proteins, so the maximum calcium channel inhibition is 50%). Fig. 3b represents the amount of non-activated (i.e. undissociated) G-protein complexes over time under the analogous conditions.

Ligand	pH = 7.4	pH = 6.5	pH = 5.5
Fentanyl	$2.5 \times 10^{-2}s^{-1}$	$1.25 \times 10^{-2}s^{-1}$	$2.5 \times 10^{-3}s^{-1}$
NFEPP	$5 \times 10^{-4}s^{-1}$	$2.5 \times 10^{-3}s^{-1}$	$2.5 \times 10^{-3}s^{-1}$

Table 1. Receptor-ligand binding rates. Rate constant k_1 for receptor activation by ligand-binding, depending on the ligand and the pH-level.

The findings from these numerical studies for the basic scenario are consistent with the results from *in vitro* experiments (see Fig. 4). Both the FRET and the patch-clamp measurements show a normal maximum effect (G-protein activation or inhibition of calcium currents, respectively) of fentanyl at all pH values and of NFEPP at low pH, but a significantly smaller effect of NFEPP at pH 7.4.

Impact of oxygen radicals and additional DSB

The pH value has an impact on the binding rate of NFEPP and fentanyl. However, we found that the receptor-ligand binding rate was also influenced by an additional DSB, which is typically promoted by increased radical concentrations (***Bowen and Pert, 1982***). In the atomistic MD simulations, the difference between inflamed and healthy tissue was modelled by changes in pH and with the formation of a DSB. In order to account for protonation and deprotonation of respective amino acid residues and ligands, the simulation parameter setting for inflamed tissue was pH 5 and the setting for healthy tissue was pH 7. As explained in the methods section, this parameter setting does not really represent a concrete H^+-ion concentration, but only has an influence on the protonation state of the MOR amino acid residues. The setting pH 7 results in the same protonation states of amino acid residues as pH 7.4 and, therefore, models the healthy tissue situation. In the rat MOR, CYS $292^{6.47}$ of the TM6 helix along with CYS $321^{7.38}$ of the neighbouring TM7 helix were selected for the introduction of an additional DSB. Sulfur atoms of these two cysteine residues are at a distance of 0.987 nm in the native rat MOR crystal structure, see Protein Data Bank (PDB) (***wwPDB consortium, 2019***), code 6DDF (***Koehl et al., 2018***). Significantly, CYS $292^{6.47}$ is also in proximity of HIS $297^{6.52}$, which is crucial for the interaction of the binding pocket of the receptor with opioid ligands (***Koehl et al., 2018***; ***Ray et al., 2020***). Hence, it is of special interest to examine ligand binding and activation of the MOR without and with the additional CYS $292^{6.47}$ – CYS $321^{7.38}$ DSB in the receptor, as depicted in Fig. 2.

Receptor-ligand interaction

The binding of an opioid ligand to the MOR occurs mainly between the two amino acids ASP $147^{3.32}$ and HIS $297^{6.52}$ (***Koehl et al., 2018***; ***Isberg et al., 2015***). The ligand positions itself between these two residues. Thus, the interaction of the binding region of the MOR with the ligand was assessed

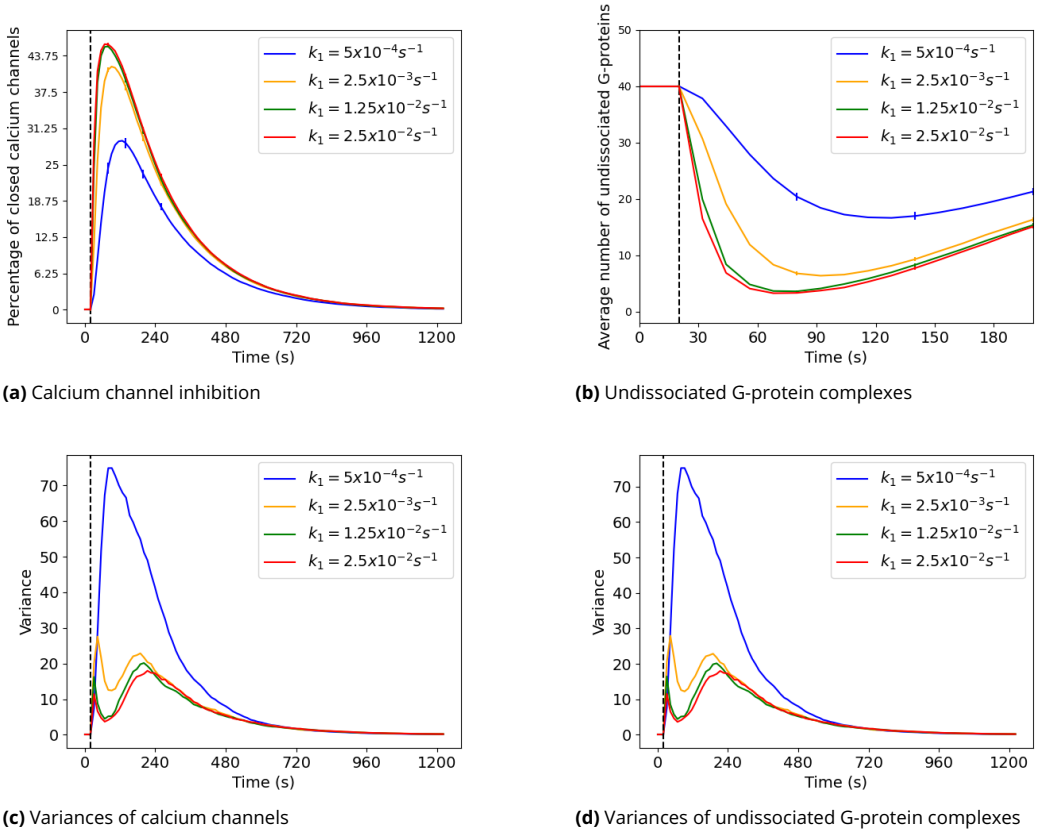

(a) Calcium channel inhibition

(b) Undissociated G-protein complexes

(c) Variances of calcium channels

(d) Variances of undissociated G-protein complexes

Figure 3. Numerical studies. (a) Time course of percentage of closed calcium channels for different values of the ligand-binding rate k_1. Note that there can be maximally 40 closed calcium channels (corresponding to 50% on the y-axis) because there are not more than 40 $\beta\gamma$-units (see Tab. 4). Error bars indicate 95%-confidence intervals (from 500 simulation runs). (b) Time course of average number of undissociated $\alpha\beta\gamma$-complexes for different k_1-values. (c) Variances of closed calcium channels from 500 simulation runs. (d) Variances of undissociated G-protein complexes from 500 simulation runs.
The dashed line indicates the time point $t = 20s$ in all figures.

by measuring its distance with regard to the crucial ASP $147^{3.32}$ and HIS $297^{6.52}$ residues of the binding region (***Ray et al., 2020***).

The formation of an additional DSB is promoted by radicals and, thus, due to the situation of inflamed tissue. In healthy tissue the formation of additional DSB is unlikely. This means, that in Fig. 5 mainly 5a and 5c are of importance. At pH 5, fentanyl exhibited similar interactions with the binding region irrespective of the additional DSB, as shown in Fig. 5a. However, the fluctuation in the receptor-ligand interaction was demonstrably higher without the extra DSB. The ligand stays in greater proximity of ASP $147^{3.32}$ as compared to HIS $297^{6.52}$. For NFEPP, interaction with the ASP $147^{3.32}$ residue at pH 5 gets affected upon the introduction of the additional DSB. However, ligand interaction with HIS $297^{6.52}$ remains similar for both scenarios (Fig. 5c). From this observation, we conclude, that the presence of an additional CYS $292^{6.47}$ – CYS $321^{7.38}$ DSB has an effect on the binding mode of opioids. An additional DSB can have a significant influence on these systems especially in the case of NFEPP. Hence, increased concentrations of radicals (which induce the formation of DSB) can indeed affect ligand binding at the MOR and perhaps the subsequent signalling events downstream. Our conclusion from the change in the atomic distances between the opioid ligands and the important binding positions is that DSB formation reduces the binding rate k_1. A similar role of DSB has been previously implicated in the modification of the ligand-access channel of cytochrome P450 2B1 (***Zhang et al., 2009***) and in the functionality of other GPCRs (***Weis and Kobilka,***

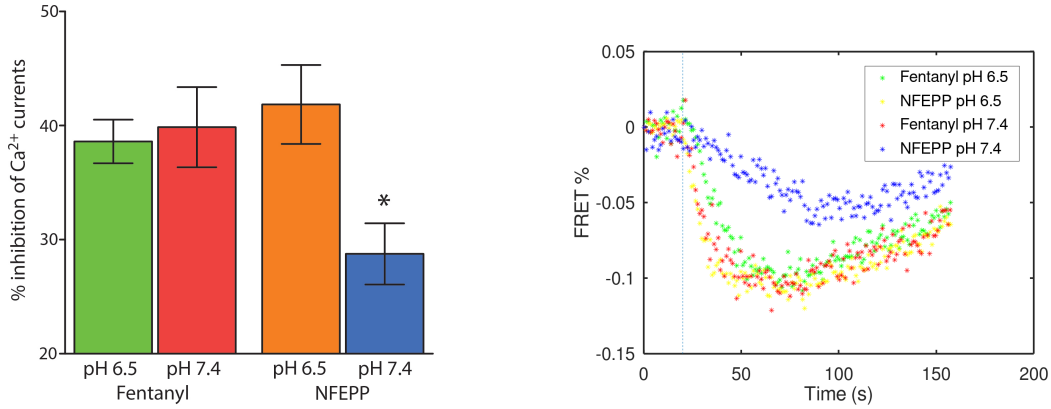

(a) Calcium currents

(b) G-protein activation

Figure 4. *In vitro* experiments. (a) Maximum inhibition of voltage-induced calcium currents by fentanyl or NFEPP at pH 6.5 and pH 7.4 measured by patch clamp experiments in rat sensory neurons. *P<0.05 NFEPP at pH 7.4 vs. all other values (one-way ANOVA with Bonferroni's multiple comparisons). Data are means ± standard error of the mean (SEM). These findings are comparable to the scenarios simulated in Fig. 3a. (b) Experimental data from (***Spahn et al., 2017***) are comparable to the scenarios simulated in Fig. 3b. The time course of ligand-induced G-protein subunit dissociation (i.e. G-protein activation) was measured by Förster resonance energy transfer (FRET). A higher number of dissociated G-protein subunits (i.e. stronger G-protein activation) is represented by more negative FRET values. One can directly see that the blue "curve" (NFEPP at pH 7.4) shows lower numbers of dissociated subunits (i.e. weaker G-protein activation) compared to the other scenarios. This is comparable to $k_1 = 5 \times 10^{-4} s^{-1}$ in Fig. 3b. The dashed line indicates the time point $t = 20s$ where the ligand was added.

2018).

In inflamed tissue, the amino acid residues are not "completely protonated". With a low probability, we also find the situations that correspond to a parameter setting of pH 7 in molecular simulations. Fentanyl would interact less with HIS $297^{6.52}$ with an additional DSB in the receptor using this parameter setting. However, the distance of the ligand from ASP $147^{3.32}$ remains similar, both without and with the extra DSB (Fig. 5b). NFEPP prefers interaction with HIS $297^{6.52}$ without the DSB, and with ASP $147^{3.32}$ if an extra DSB would be present at pH 7 (Fig. 5d). This again shows that a lower rate constant k_1 can be expected in the case of DSB formation.

Constitutive G-protein dissociation

The TM6 of the MOR is known to play a crucial role in ligand binding. Furthermore, the outward movement of TM6 is the largest structural change upon receptor activation (***Weis and Kobilka, 2018***). The position of TM6 may change just because of the presence of an additional DSB, even if a ligand is not bound. Changes in the MOR conformation were monitored by tracking the distance between the TM6 and TM7 helices in MD simulations without a ligand, as depicted in Fig. 6. The additional CYS $292^{6.47}$ – CYS $321^{7.38}$ DSB causes a reduction in the distances between these two helices by approximately 0.1 nm at both pH 5 and 7. Hence, a conformational change of MOR might occur in inflamed tissue, as the surrounding environment turns more acidic accompanied by increased radical concentrations, which can trigger formation of DSB (***Bowen and Pert, 1982***).

From our MD simulations we see that the position of TM6 depends on several extracellular factors. It is to be expected that the spontaneous (constitutive) dissociation of G-protein subunits is influenced by conformational changes of TM6. So our MD simulations imply that we have to extend our reaction network to include the possible influence of DSB on constitutive activity. What kind of influence can be expected from *in vitro* data? The formation of DSB is chemically based on reactive oxygen species (***Bowen and Pert, 1982***). These species can be produced in *in vitro* experiments by adding H_2O_2 to the sample. Our experimental data support that increasing radical (H_2O_2) concentrations (likely associated with increasing DSB formation) are correlated with increas-

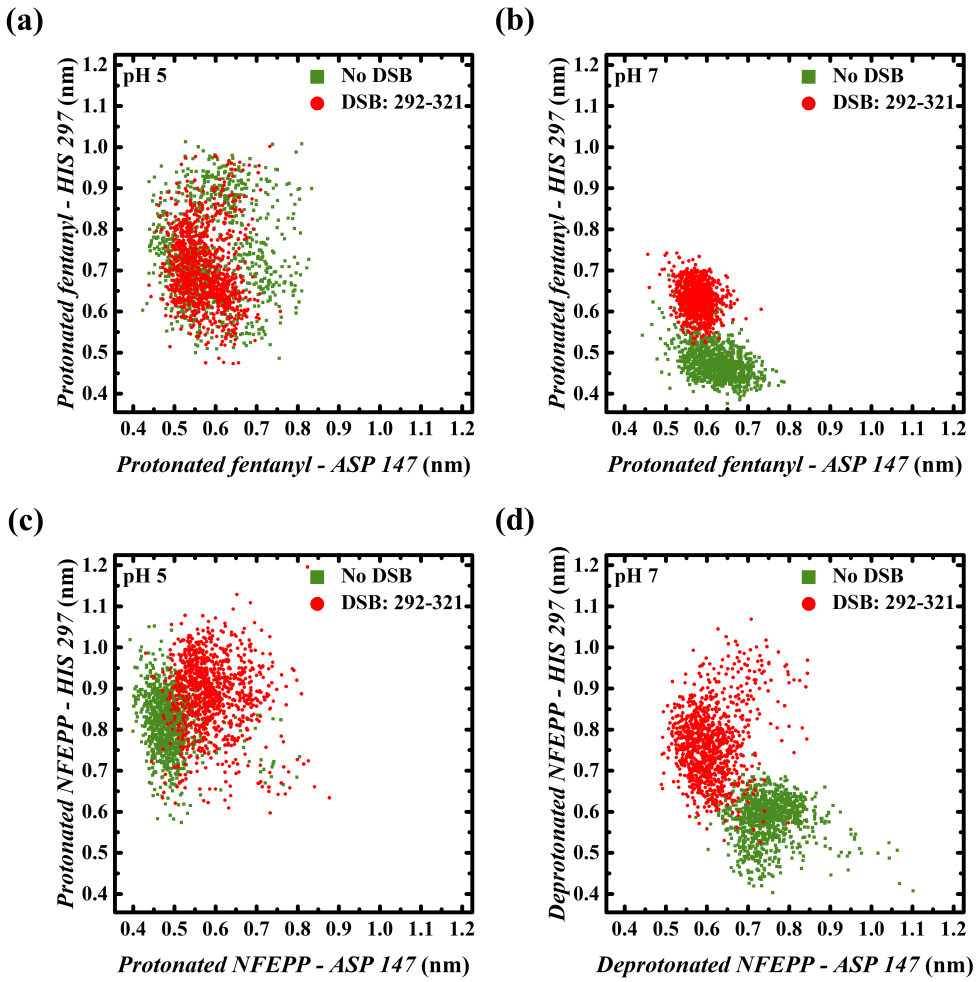

Figure 5. Receptor-ligand interaction. Distance distributions of fentanyl (a, b) and NFEPP (c, d) as a function of system acidity, with respect to the ASP 147$^{3.32}$ and HIS 297$^{6.52}$ residues of the binding region. System states without and with an additional CYS 292$^{6.47}$ – CYS 321$^{7.38}$ DSB are represented by green filled-squares and red filled-circles, respectively.

ing constitutive receptor activity (i.e. G-protein activation) (Fig. 7).

In order to take this constitutive G-protein activation into account, we extended the basic reaction network by a spontaneous activation of the receptor independently of ligands (see reaction $\mathcal{R}_{11}$ in Tab. 2). For our studies, the rate k_{11} of this additional reaction was modified in order to understand the effect of additional DSB onto the reaction cascade. The results of these studies are presented in the following subsection.

Parameter studies for extended model

We next investigated the effect of rising radical levels (accompanied by additional DSB in the receptor) onto the dynamics. The results from the MD simulations described before showed a decrease of the receptor-ligand binding rate k_1 and an increase in constitutive G-protein activation modelled with rate k_{11}. The introduction of constitutive receptor activation now leads to a higher baseline level of closed calcium channels depending on the rate of constitutive receptor activation. This level was evaluated in a preliminary simulation run without ligand, and the initial state was adjusted for each value of k_{11} accordingly. With progressive inflammation, there are now two effects on k_1, one from the lower pH and one from more DSB. We assumed that the DSB effect decreases k_1 to about 80% at pH 6.5, and to about 70% at pH 5.5. For fentanyl, k_1 decreases due to both pH and DSB, while

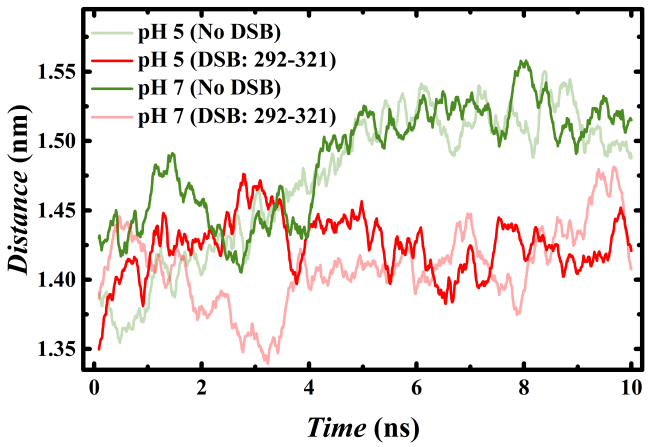

Figure 6. MOR conformation. Time evolution of distance between TM6 and TM7 helices as a function of system pH values of 5 and 7, and absence (green) or presence of an additional CYS 292$^{6.47}$ – CYS 321$^{7.38}$ DSB (red). Physiologically relevant and relatively transient states are represented by solid and faded lines, respectively.

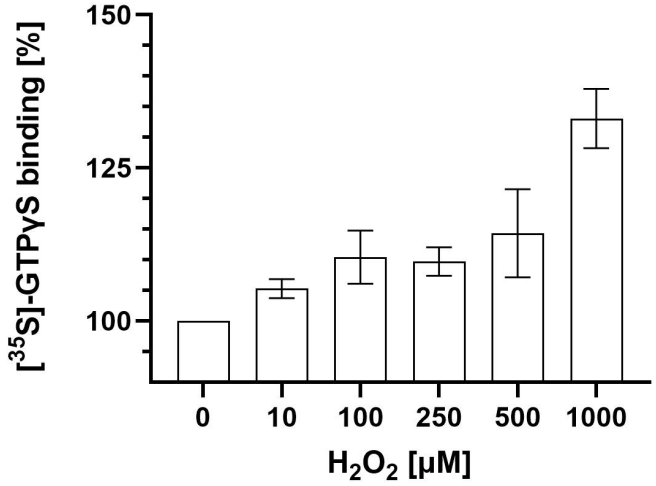

Figure 7. Constitutive receptor activity. Effects of increasing concentrations of radicals (H_2O_2) on basal [^{35}S]-GTPγS binding to MOR without opioid ligands. Data are means ± SEM of specific binding normalised to the control group; n=8 per condition. P<0.05, linear regression analysis.

for NFEPP, k_1 increases due to pH and decreases due to DSB. Without ligands, constitutive receptor activity increases with progressive inflammation (i.e. rising radical concentrations). This is seen in Fig. 8 which shows two plots, one for fentanyl and one for NFEPP. The black curve represents the healthy tissue situation (pH 7.4, no DSB) while the olive (pH 6.5, some DSB) and orange (pH 5.5, more DSB) curves show the effects of progressive inflammation. The change of k_1 has the already known effect of reducing the amplitude of the closed calcium channels which is not altered by the constitutive receptor activity. Increasing k_{11} results in a rising number of closed calcium channels.

Discussion

We present a stochastic model of a canonical GPCR signalling pathway linked to plasma membrane function. This pathway is composed of a biochemical reaction network which begins at the receptor, continues with the G-protein and extends to the membrane calcium channels. In addition, we have studied the functional role of DSB inside the binding pocket. Our modelling results regarding

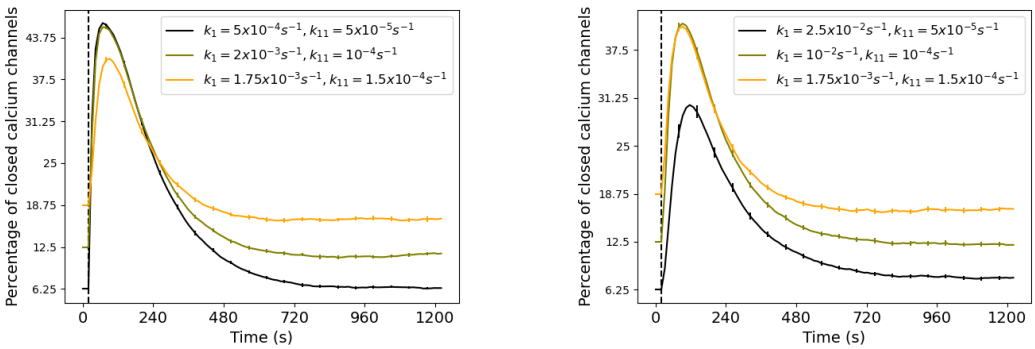

(a) Fentanyl **(b)** NFEPP

Figure 8. Effects of ligand-binding rate k_1 and constitutive activation rate k_{11}. Time course of percentage of closed calcium channels for different k_1- and k_{11}-values for the ligands fentanyl and NFEPP. Black curves represent the healthy tissue situation, while olive and orange show the effects of progressively more inflammation (lower pH, more receptors with DSB). The time axis is the same as in Fig. 3a. Error bars indicate 95%-confidence interval (for 500 simulation runs). The dashed lines indicate the time point $t = 20s$ in all figures.

calcium channels and G-protein activation were validated by *in vitro* experiments.

Initially, we show that the change in reaction rates translates into a markedly diminished effect (i.e. a lower number of closed calcium channels) of NFEPP at normal pH compared to all other scenarios (NFEPP at low pH, fentanyl at low or normal pH). The model shows a non-linear behaviour of the calcium channel inhibition response with regard to the change of the receptor-ligand binding rate k_1. For the chosen parameter setting, a critical value of k_1 at which the response drops markedly, is $k_1 = 5x10^{-4}s^{-1}$ (corresponding to $k_1 = 0.01$ in the unitless regime, see Fig. 1 in the appendix, where the probability of no receptor-ligand binding can be seen as a surrogate parameter for a low amount of closed calcium channels). These results support our previous studies demonstrating that the conventional ligand fentanyl activates MOR both in injured (low pH) and non-injured (normal pH) tissues, while NFEPP is not active in non-injured environments (brain, intestinal wall) (***Spahn et al., 2017***; ***Rodriguez-Gaztelumendi et al., 2018***; ***Massaly et al., 2020***; ***Jimenez-Vargas et al., 2021***). In contrast to an ordinary differential equation model we were able to investigate this phenomenon further and can state that this decrease is not due to a uniform decrease of all trajectories but to a stronger decrease of some trajectories and the nearly unchanged course of others. Mathematically, this is represented by the rise of the variance of trajectories (see Fig. 3c).

To find out about the effect of additional DSB, a two stage approach was used: As a first step, qualitative changes of the reaction rates were assessed by MD simulations, and as a second step, these rates were used for stochastic simulations of the corresponding reaction jump process. The MD simulations with DSB imply a decrease of k_1, the amount of which is hard to quantify. With the amount of decrease we assumed in the extended model parameter study section, no decisive changes in the effect of both ligands are to be expected. Only if one assumes the decrease to be large enough to drop k_1 below the critical value of $5x10^{-4}s^{-1}$, marked changes will be seen. At low pH (5.5), a decrease towards the critical value may be possible for either fentanyl or NFEPP. Also, evidence for a relatively higher constitutive receptor activity could be deduced from our MD simulations which were validated by *in vitro* experiments. Absolute values cannot be inferred from the current state of our research. The testing of several combinations of binding rates and constitutive activation levels showed no large mutual influences.

These results are an extension of the findings in our earlier work (***Spahn et al., 2017***). There it was theorised and corroborated in animal studies that a ligand with proper pH-dependent bind-

ing rate would exhibit analgesic effects without side effects. Now we can add that the change of binding rates results in reduced calcium channel inhibition. Thus, the present data provide a more detailed explanation by including the intracellular signalling pathway underlying our initial findings. This further supports our concept of targeting disease-specific conformations of MOR to preclude adverse side effects of painkillers.

With regard to other inflammatory mediators (radicals), our study implies lower binding rates of fentanyl and NFEPP, and a higher constitutive activity of the MOR after introducing a new DSB between TM6 and TM7 inside the binding pocket. The role of DSB in GPCR has also been investigated by others. For example, ***Zhang et al.*** (***1999***) describe decreased ligand binding after the removal of a DSB in the extracellular part of the MOR. A review article by ***Wheatley et al.*** (***2012***) mentions decreased agonist affinity at the CXC-chemokine receptor 4 and increased constitutive activity of the angiotensin II type 1 receptor after breaking extracellular DSBs. It must be kept in mind that ligands may cleave extracellular DSB in MOR (***Brandt et al., 1999***). If this also occurs inside the binding pocket, radical-induced DSB formation may not play a major role for opioid receptor activity.

In summary, comparing the influence of two prominent inflammatory mediators (pH and radicals) on ligand-induced opioid receptor function, it seems that pH has a higher impact than radicals under the chosen parameters. When designing novel opioid painkillers devoid of side effects elicited in non-injured environments, pH-sensitivity may be more important than radical-sensitivity. Given the high degree of homology between GPCRs (***Congreve et al., 2020***), our current studies may be applicable to other signalling pathways (e.g. from receptor to nucleus (***Shaw et al., 2019***)), to GPCR involved in other diseases (e.g. cancer, high blood pressure, addiction, depression, arthritis) or even to non-human GPCRs in deranged environments (e.g. in animals or plants exposed to ocean acidification).

Materials and Methods

Reaction network: Stochastic model

The basic biochemical reaction network under consideration consists of the following reactions (see Tab. 2 for an overview and Fig. 1 for an illustration). A ligand L attaches to a receptor R in the membrane, resulting in a receptor-ligand complex RL (reaction $\mathcal{R}_1$). This receptor-ligand complex RL activates a trimeric G-protein complex which leads to exchange of GDP by GTP and subsequent dissociation into α- and $\beta\gamma$-subunits (reaction $\mathcal{R}_2$). These subunits activate different signalling pathways. Along with the hydrolysis of GTP, another reaction partner M (e.g. arrestin) emerges (reaction $\mathcal{R}_3$), which initiates internalisation of the receptor-ligand complex (reaction $\mathcal{R}_4$). The $\beta\gamma$-subunit inhibits a membrane calcium channel by binding to it (reaction $\mathcal{R}_5$). After dissociation of the $\beta\gamma$-subunit from the calcium channel, a trimeric G-protein complex is reformed, and the calcium channel is opened (reaction $\mathcal{R}_6$). The internalised receptor RL_w is either recycled to the cell membrane (reaction $\mathcal{R}_7$) or degraded (reaction $\mathcal{R}_8$). The reaction partner M can itself be degraded (reaction $\mathcal{R}_9$). The ligand L can vanish before it binds to the receptor, e.g. by degradation or unspecific binding to other extracellular components (reaction $\mathcal{R}_{10}$), or it is degraded intracellularly (reactions $\mathcal{R}_7$ and $\mathcal{R}_8$). In the extended reaction network, we added a reaction $\mathcal{R}_{11}$, which represents a spontaneous (constitutive) activation of the receptor by simply using $\mathcal{R}_2$ without ligand.

The state of the system is given by a vector

$$\boldsymbol{x} = (x_L, x_R, x_{RL}, \ldots) \in \mathbb{N}_0^{11}$$

counting the number x_S of molecules of the different species $S \in \mathcal{S}$, where $\mathcal{S}$ is the set of species under consideration:

$$\mathcal{S} := \left\{ L, R, RL, RL_w, \alpha_{GDP}\beta\gamma, \alpha_{GDP}, \alpha_{GTP}, \beta\gamma, M, Ca_{\mathrm{On}}, Ca_{\mathrm{Off}} \right\}.$$

For each reaction $\mathcal{R}_j$ there is a stoichiometric vector $\boldsymbol{\nu}_j \in \mathbb{Z}^{11}$ defining the net change in the population state $\boldsymbol{x}$ induced by this reaction. That is, each time that reaction $\mathcal{R}_j$ occurs, this leads to a

j	Reaction $\mathcal{R}_j$	Propensity f_j
1	$L + R \xrightarrow{k_1} RL$	$k_1 \cdot x_R \cdot x_L$
2	$RL + \alpha_{GDP}\beta\gamma \xrightarrow{k_2} RL + \alpha_{GTP} + \beta\gamma$	$k_2 \cdot x_{RL} \cdot x_{\alpha_{GDP}\beta\gamma}$
3	$\alpha_{GTP} \xrightarrow{k_3} \alpha_{GDP} + M$	$k_3 \cdot x_{\alpha_{GTP}}$
4	$RL + M \xrightarrow{k_4} RL_w$	$k_4 \cdot x_{RL} \cdot x_M$
5	$\beta\gamma + Ca_{\text{On}} \xrightarrow{k_5} Ca_{\text{Off}}$	$k_5 \cdot x_{\beta\gamma} \cdot x_{Ca_{\text{On}}}$
6	$\alpha_{GDP} + Ca_{\text{Off}} \xrightarrow{k_6} \alpha_{GDP}\beta\gamma + Ca_{\text{On}}$	$k_6 \cdot x_{\alpha_{GDP}} \cdot x_{Ca_{\text{Off}}}$
7	$RL_w \xrightarrow{k_7} R$	$k_7 \cdot x_{RL_w}$
8	$RL_w \xrightarrow{k_8} \emptyset$	$k_8 \cdot x_{RL_w}$
9	$M \xrightarrow{k_9} \emptyset$	$k_9 \cdot x_M$
10	$L \xrightarrow{k_{10}} \emptyset$	$k_{10} \cdot x_L$
11^*	$R + \alpha_{GDP}\beta\gamma \xrightarrow{k_{11}} R + \alpha_{GTP} + \beta\gamma$	$k_{11} \cdot x_R \cdot x_{\alpha_{GDP}\beta\gamma}$

Table 2. Reactions and propensities. R: receptor, L: ligand, RL: receptor-ligand complex, RL_w: internalised receptor, $\alpha_{GDP}\beta\gamma$: G-protein, $\alpha_{GDP}/\alpha_{GTP}$: α-subunit loaded with GTP or GDP, respectively, $\beta\gamma$: $\beta\gamma$-subunit, M: reaction partner (e.g. arrestin) to initiate receptor internalisation, $Ca_{\text{Off}}/Ca_{\text{On}}$: closed/open calcium channel. Reaction $\mathcal{R}_{11}^*$ was used only when the effect of radicals was modelled (extended reaction network). For any species S it stands x_S for the number of molecules of this species.

jump in the system's state of the form

$$\boldsymbol{x} \mapsto \boldsymbol{x} + \boldsymbol{\nu}_j.$$

E.g., the stoichiometric vector $\boldsymbol{\nu}_1$ of reaction $\mathcal{R}_1$ is given by $\boldsymbol{\nu}_1 = (-1, -1, 1, 0, ..., 0)$. The rates at which the reactions occur are given by propensity functions $f_j : \mathbb{N}_0^{11} \to [0, \infty)$, which can be found in the right column of Tab. 2.

The temporal evolution of the system is described by the Markov jump process $(\boldsymbol{X}(t))_{t\geq 0}$, $\boldsymbol{X}(t) = (X_S(t))_{S\in\mathcal{S}}$, where $X_S(t)$ is the number of molecules of species S at time t. We define the probability $p(\boldsymbol{x}, t) := \mathbb{P}(\boldsymbol{X}(t) = \boldsymbol{x} | \boldsymbol{X}(0) = \boldsymbol{x}_0)$ to find the system in state $\boldsymbol{x}$ at time t given some initial state $\boldsymbol{x}_0$. Then, the overall dynamics are characterised by the standard chemical master equation (***Gillespie, 1992***; ***Winkelmann and Schütte, 2020***) given by

$$\frac{d}{dt}p(\boldsymbol{x}, t) = \sum_{j=1}^{n} \left[f_j(\boldsymbol{x} - \boldsymbol{\nu}_j)p(\boldsymbol{x} - \boldsymbol{\nu}_j, t) - f_j(\boldsymbol{x})p(\boldsymbol{x}, t), \right]$$

where n is the number of reactions under consideration (i.e., $n = 10$ in the basic scenario and $n = 11$ in the extended scenario).

We simulated the stochastic process $(\boldsymbol{X}(t))_{t\geq 0}$ via the Gillespie algorithm (***Gillespie, 1977***) for different scenarios represented by different rate values. Only the rates k_1 and k_{11} have been altered, while the rate constants for reactions $\mathcal{R}_2, ..., \mathcal{R}_{10}$ were left unchanged. The respective values are given in Tab. 3. We started by setting the rate $k_5 = 1$ as the rate of the central binding reaction of the $\beta\gamma$-subunit to the calcium channel and proceeded to arrange the other values relative to it according to what is known in the literature. From ***Zamponi and Snutch*** (***1998***) it can be deduced that $\mathcal{R}_5$ happens at a level of hundreds of milli-seconds while from ***Shea et al.*** (***2000***) we know that $\mathcal{R}_2$ and $\mathcal{R}_3$ happen at a level of seconds, so we chose k_2 and k_3 ten times smaller than k_5. The rates of reactions $\mathcal{R}_1, \mathcal{R}_4, \mathcal{R}_6, \mathcal{R}_9$ were assumed to be of the same magnitude as those of $\mathcal{R}_2, \mathcal{R}_3$. The recycling and degradation of internalised ligand-receptor complexes are much slower, at a level of minutes (Fig. 1 in ***Williams et al.*** (***2013***)) which leads to comparatively small rate constants k_7 and k_8 for the reactions $\mathcal{R}_7$ and $\mathcal{R}_8$ of the internalised receptor. The extracellular decay of ligand due to unspecific binding and other incidents (reaction $\mathcal{R}_{10}$) was set to a value at which it showed a first effect on calcium channel inhibition, with $k_1 = 0.01$. Constitutive receptor activity, which is represented by the rate k_{11} of reaction $\mathcal{R}_{11}$, was set to show a base level of approximately 5 closed

calcium channels in the healthy tissue scenario, which appears to be a reasonable value compared to the other model parameter values.

After running the model with these parameters which gave a unitless time axis since the rate constants are unitless, we compared the results with the time course of the findings of the *in vitro* experiments. We found that by scaling our rate constants with a factor $c = (20s)^{-1}$ and thereby indirectly the time axis of our simulations, we could fit both time courses (*in vitro* and simulation) accordingly. So the rates from table 3 were finally multiplied by c to equip the simulation time axis with the unit seconds.

k_1	k_2	k_3	k_4	k_5	k_6	k_7	k_8	k_9	k_{10}
see Tab. 1	0.2	0.1	0.1	1	0.5	0.01	0.001	0.1	0.5

Table 3. Reaction rate constants. Chosen values for the rate constants of the basic scenario.

Simulations were made with Python 3. For each combination of rate constants, 500 Monte Carlo simulations were carried out and the arithmetic mean was calculated in order to estimate the percentage of closed calcium channels plotted in Fig. 3 and Fig. 8. As a time horizon for each simulation 1200 seconds were chosen. For all simulations of the basic model the initial state in Tab. 4 was used. To check for normal distribution of the mean, the 500 runs were divided into batches of 50 and the respective means then tested. Anderson-Darling test indicated normal distribution with $p \leq 0.05$, so the 95%-confidence interval of the t-distribution is shown in the plots.

For the extended model the initial state was adapted according to the new baselevel of constitutive receptor activation. The same procedure as in the basic model was carried out to ensure normal distribution of the means.

Species S	L	R	RL	RL_w	$\alpha\beta\gamma$	α_{GDP}	α_{GTP}	$\beta\gamma$	M	Ca_{On}	Ca_{Off}
$X_S(0)$	10	20	0	0	40	0	0	0	0	80	0

Table 4. Initial state. Initial number $X_S(0)$ of molecules for each species $S \in \mathcal{S}$ used for all simulations.

MD simulations

For creating the different possible protonation states of the MOR amino acid residues in inflamed and in healthy tissue in the computational molecular model, a virtual "pH" value has to be selected. In inflamed tissue we selected "pH 5", in healthy tissue "pH 7". This only accounts for the modelling of protonated vs. deprotonated amino acids, because individual H^+-ions are not part of the modelling. In reality, we always will find a mixture between different protonation states of amino acids. For example, at normal pH 7.4 there is also a small percentage of protonated histidines. Thus, in the following passages "pH 5" and "pH 7" just accounts for the parameter setting during the modelling step. Furthermore, the argument that there is always a mixture of different states also led us to take into account transient states with an additional DSB at pH 7 and without an additional DSB at pH 5. Systems at pH 5 and pH 7 without a ligand were also considered, both without and with an additional DSB, for comparison with systems where a ligand was present in the vicinity of the binding region.

For molecular modelling, the rat MOR structure was procured from the RCSB database (Protein Data Bank (PDB): 6DDF). Protonation states of the individual amino acid residues in the receptor were determined based on calculations at pH 5 and pH 7. The histidine imidazole side-chain has a pKa value of 5.97 (***Williams, 2013***). Hence, these two levels of system acidity represent histidine states below (pH 5) and above (pH 7) the side-chain pKa. Other amino acids retain their protonation states as observed at normal pH (7.4). The protonated form of fentanyl, and the protonated and deprotonated forms of NFEPP (***Spahn et al., 2017***) were sketched and parameterised using the CHARMM-GUI *Ligand Reader & Modeler* (***Kim et al., 2017***). The protonated fentanyl was positioned

onto the MOR at pH 7 with the Autodock program (**Morris et al., 2009**). The docking calculations employed the Gasteiger-Marsili charges (**Gasteiger and Marsili, 1978**). Autogrid was used for grid preparation, with grid spacing set to 0.65 Å to cover the entire receptor. Lamarckian genetic algorithm (**Morris et al., 1998**) was used to perform ten docking runs; with the rates of gene mutation and crossover kept at 0.02 and 0.8, respectively for the LUDI scoring function employed (**Böhm, 1994**). Remaining docking parameters were kept at their default values. The receptor-ligand complex with most energetically-favourable docking was used for further simulations. For similar starting conformations, the other ligands were aligned to the docked protonated fentanyl with the *RMSD Trajectory Tool* of VMD (**Humphrey et al., 1996**).

The receptor-ligand complexes were inserted into the 1-palmitoyl-2-oleoyl-sn glycerol-3-phosphatidyl choline (POPC) bilayer models using the CHAMM-GUI *Membrane Builder* (**Lee et al., 2019**). Similar to (**Ray et al., 2020**), MD simulations were performed with GROMACS 2019.6 (**Abraham et al., 2015**), using the CHARMM36m force-field for the ligands (**Soteras Gutiérrez et al., 2016**), receptor (**Huang et al., 2017**) and lipids (**Klauda et al., 2010**). The CHARMM TIP3P water model (**Jorgensen et al., 1983**) was used as an explicit solvent. Sodium and chloride counterions were added to neutralise the excess charge and obtain a salt concentration of 0.15 M. The particle mesh Ewald (PME) method (**Essmann et al., 1995**) was employed to calculate long-range Coulombic interactions, with a 1.2 nm cut-off for real-space interactions. A force-switch function was implemented for the Lennard-Jones interactions, with a smooth cut-off from 1.0 to 1.2 nm. The temperature was maintained at 310 K using the Nosé-Hoover thermostat (**Nosé, 1984**; **Hoover, 1985**). System pressure was kept at 1 bar with the Parrinello-Rahman barostat (**Parrinello and Rahman, 1981**), using a semi-isotropic scheme where pressure along x-y-directions and the z-direction were coupled separately. Coupling constant and compressibility of the barostat were set to 5 ps and 4.5×10^{-5} bar, respectively. The LINCS algorithm (**Hess et al., 1997**) was used to constrain the covalent bonds between hydrogen and other heavy atoms, allowing a simulation time-step of 2 fs.

All simulation systems went through consecutive minimisation, equilibration and production runs, using the GROMACS scripts generated by the CHARMM-GUI (**Lee et al., 2019**). First, the systems were energy minimised with steepest descent algorithms, followed by six-step equilibration runs. The first two runs were performed in the NVT (constant particle number, volume, and temperature) ensemble and the remaining runs in the NPT (constant particle number, pressure, and temperature) ensemble. Restraint forces were applied to the ligand, receptor, lipids, and water molecules, and z-axis positional restraints were placed on lipid atoms to restrict their motion along the x-y-plane. These restraints were progressively reduced during the equilibration process. Additional restraints were applied throughout equilibration to keep the distance between the crucial ASP $147^{3.32}$ and HIS $297^{6.52}$ residues of the MOR binding site (**Ray et al., 2020**) and the ligand molecule to the minimum possible. This ensured similar receptor-ligand starting conformations for the production runs of all the systems. Ultimately, unrestrained NPT production runs of 10 ns were performed, with periodic boundary conditions along all three orthonormal directions. Production run trajectories were saved every 10 ps, and processed with GROMACS analysis tools to generate the required information. VMD software was used for visualisation.

In vitro experiments

Measurement of calcium currents in sensory neurons

To mimic the mechanisms underlying *in vivo* opioid analgesia, we examined calcium currents in sensory neurons harvested from rodents using a patch clamp protocol modified from (**Walwyn et al., 2007**). The following chemicals were used: Dulbecco's Modified Eagles Medium (DMEM)/HAM's F-12 medium (Biochrom F4815, Berlin, Germany), Penicillin (10,000 U), Streptomycin (10 mg/ml), 1.25% Collagenase (Sigma-Aldrich C0130, Taufkirchen, Germany), 2.5% Trypsin (Sigma-Aldrich T0303), acridine orange/propidium iodide (Logos, Villeneuve, France), $CaCl_2 \cdot 6H_2O$, TEA-Cl_2, 4-(2-hydroxyethyl)-1-piperazineethanesulfonic acid (HEPES), d-glucose, CsCl, $MgCl_2$, ethylene glycol-bis-(β-aminoethyl ether)-N,N,N',N'-tetraacetic acid (EGTA), Mg-ATP, GTP (Sigma-Aldrich).

Dorsal root ganglia (DRG) were harvested from naïve male Wistar rats (200-300 g; Janvier, Le Genest-Saint-Isle, France). Rats were killed by an overdose of isoflurane (AbbVie, Wiesbaden, Germany). The thoracic and lumbar spinal regions were exposed, DRG were collected in a digestive solution with 1.25% collagenase and incubated for 60 min at 37°C. After washing the cells three times with phosphate buffered saline (PBS), they were incubated in a digestive solution with trypsin for another 10 min at 37°C. After digestion, the tissue was triturated using plastic pipette tips and subsequently filtered through a 40 μl filter. The filtrate was centrifuged, the supernatant was discarded and the pellet was resuspended in 1 ml culture medium (DMEM/HAM's F12 supplemented with 1% penicillin/streptomycin and 10% horse serum). Cells were then seeded onto poly-L-lysine coated plastic culture dishes (35 mm) and placed in an incubator (5% CO_2 at 37°C). One hour later, the cell cultures were topped up to a total of 2 ml of culture medium and cultured until patch clamp recordings, as previously described (***Nockemann et al., 2013***).

Recordings from DRG neurons were performed 24–48 h after plating. Cell viability was evaluated before the first experiment by an automated cell counter (Luna, Villeneuve, France) using acridine orange/propidium iodide. Recordings were carried out in whole-cell voltage clamp mode. After washing with PBS, cells were bathed in an extracellular buffer (ECS) (10 mM $CaCl_2 \cdot 6H_2O$, 130 mM TEA-Cl_2, 5 mM HEPES, 25 mM d-glucose; adjusted to pH 7.4 or 6.5; all from Sigma-Aldrich) and visualised using a Zeiss Axiovert 200 inverse microscope (Zeiss, Jena, Germany). Patch pipettes (resistance 3.5–8 MΩ) were produced from Borosilicate glass capillaries using a Sutter P-97 puller (Sutter Instruments, Novato, CA, USA) and filled with intracellular buffer (105 mM CsCl, 2.5 mM $MgCl_2$, 40 mM HEPES, 10 mM EGTA, 2 mM Mg-ATP, 0.5 mM GTP, 5 mM d-glucose; adjusted to pH 7.4 or 6.5; all from Sigma-Aldrich). Currents were amplified and recorded using an EPC-10 patch amplifier and Pulse software (HEKA, Lambrecht, Germany). Extracellular buffer was added in a steady flow of 800–1,000 μl/min using a pressurised application system (Perfusion Pressure Kit VPP-6; Warner Instruments, Hamden, CT, USA) and a suction pump. Opioid ligands (fentanyl, NFEEP, naloxone) were applied using a perfusion valve system (VC-6; Warner Instruments) to switch between vehicle (buffer) and the test compounds. After reaching the "giga-seal" at -60 mV, the membrane patch was breached to achieve whole-cell configuration. Only cells showing proper action potentials were selected for further experiments. The currents were initially recorded at a holding potential of -80 mV in ECS buffer in the absence of opioid ligands. Immediately thereafter, the cells were depolarised to +10 mV (100 ms) for eight times after 20 s intervals. During the first five cycles, only ECS was applied. On the sixth cycle, an opioid agonist (fentanyl, NFEPP) was added to the solution. During the last two cycles, the opioid antagonist naloxone was used to remove the agonist. All recordings were performed at room temperature.

Measurement of G-protein activation

Because these experiments require genetic alteration (by transfection) of cells, we performed these measurements in commonly used human embryonic kidney (HEK293) cells (RRID:CVCL 0045, German Collection of microorganisms and Cell Cultures, Braunschweig, Germany). All chemicals were purchased from Sigma-Aldrich (Taufkirchen, Germany), unless otherwise stated. [^{35}S]-guanosine-5'-O-(3-thio)-triphosphate ([^{35}S]-GTPγS) was purchased from Perkin Elmer (Waltham, USA). Cell culture reagents were purchased from Biochrom (Berlin, Germany).

Cells were maintained in DMEM supplemented with fetal bovine serum (Biochrom), penicillin (100 U/ml, Biochrom) and streptomycin (100 μg/ml, Biochrom) with or without geneticin (G418, 100 μg/ml, Biochrom), in 5% CO_2 at 37 °C as described before (***Spahn et al., 2017***). Cells were passaged 1:3 - 1:20 every second to third day from p8 and p28 depending on confluence. Cells were plated on culture dishes coated with poly-L-lysine 24 h before transfection. 24 h after seeding, confluent cells (70-90%) were transfected with 1 μg per 200 μl transfection mix of each plasmid containing the different cDNAs using X-tremeGENE HP DNA Transfection Reagent (Roche, Mannheim, Germany) following the manufacturer's instructions. For stable transfection, pcDNA^{TM}3.1+ carrying the rat MOR provided by Christian Zöllner (University Hamburg, Germany) was linearised with re-

striction enzyme Bg1II (NEB, Frankfurt, Germany), and linearisation was verified by agarose gel electrophoresis. After 48 h, the medium containing the transfection reagent was removed and replaced by complete DMEM with 10% fetal bovine serum and penicillin/streptomycin (100 U/ml). Successfully transfected cells were selected by adding G418 (500 μg/ml) into medium that was renewed every 2 to 3 days. Monoclonal cell lines were then created 17 days post transfection by picking single colonies of stably transfected cells using a 100 μl pipette and transferring them to poly-L-Lysine coated wells of a 96-well plate. Cells were grown to confluence and successively transferred to larger culture flasks in the continued presence of 500 μg/ml G418. Antibiotic concentration was reduced to 100 μg/ml when the cells were moved to 75 cm^2 culture flasks. Monoclonal cell lines were further characterised based on immunocytochemistry, MOR mRNA expression, subjective impression of cell growth and overall cell morphology, as described previously (***Spahn et al., 2017***). Stably transfected cell lines were cultured for a maximum of 23 passages.

Protein concentrations were determined with the Bradford assay using Coomassie Brilliant Blue G-250 dye (Bio-Rad Laboratories GmbH, München, Germany) that shifts absorption from 465 to 595 nm upon binding to proteins. The relationship between measured absorbance and protein concentration was established based on a standard curve obtained from fixed protein solutions of known composition and concentration. These measurements were performed in duplicates using Bio-Rad Protein Assay Dye Reagent Concentrate with Bio-Rad Protein Assay Standard II (Bio-Rad). Samples with unknown concentrations, standards and dye reagent concentrate were diluted according to the manufacturer's instructions, thoroughly mixed, and incubated for 5 min at room temperature. Absorption at 595 nm was measured in triplicates with a spectrophotometer. Generation of linear standard curves and interpolation of total protein concentration was performed by the device's inbuilt software. A standard curve was generated for every experiment.

Membrane fractions were prepared from transfected HEK293 cells as described previously (***Zöllner et al., 2003***). The cells were grown in 175 cm^2 tissue culture flasks to approximately 90% confluence. Cells were then washed with Tris buffer (50 mM, Trizma preset crystals, pH 7.4; Sigma Aldrich), harvested with a scraper, homogenised using a mechanical disperser (Dispergierstation T8.10, IKA-Werke, Staufen, Germany) at maximum speed for 10 s and centrifuged at 42K×g for 20 min at 4°C (Avanti JXN-26 ultracentrifuge, Beckmann Coulter, Krefeld, Germany). Cellular pellets including membranes with embedded and anchored proteins were then resuspendend in Tris buffer for washing to separate them from cytosolic components by homogenisation and centrifugation at the same settings. Supernatants were discarded and the pellets were stored at -80 °C. On the day of usage, the pellets were thawed on ice in Tris buffer and homogenised. Total protein concentrations were determined as described above and homogenates were split according to the number of conditions tested in respective assay buffers.

The [^{35}S]-GTPγS binding assay was used to determine basal G protein activation (as reflected by the exchange rate of GDP for GTP) at different H_2O_2 concentrations (0-1,000 μM). GTP was replaced by a high concentration of [^{35}S]-GTPγS in the assay solvent, and the accumulation of [^{35}S]-GTPγS-bound G proteins in the membrane was measured. Membrane fractions were prepared with the following modifications: Membranes were homogenised and dissolved in HEM G-protein buffer containing 8 mM HEPES, 8 mM 4-(2-Hydroxyethyl)-1-piperazinepropanesulfonic acid (EPPS), 8 mM 2-(N-Morpholino)-ethanesulfonic acid (MES), 100 mM NaCl, 0.2 mM EGTA, 5 mM $MgCl_2$ at pH 7.6, including freshly added 0.1% (w/v) bovine serum albumin (BSA). The desired amount of H_2O_2 was then added. To avoid interference with reactive oxygen species, the reducing agent dithiothreitol (DTT) (as originally used in (***Zöllner et al., 2003***)) was omitted. Basal [^{35}S]-GTPγS binding was assessed in the presence of vehicle without opioid ligands. In analogy to (***Ludwig et al., 2003***), 50 μg of membrane fractions in duplicates were incubated with GDP (30 μM) and [^{35}S]-GTPγS (0.05 nM) for 90 min at 30 °C. Unspecific [^{35}S]-GTPγS binding in the presence of non-radioactive GTPγS (10 μM) was subtracted to yield specific binding. Bound and free ligands were separated by rapid filtration under vacuum through Whatman GF/B glass fiber filters soaked in water followed by 6 washes with Tris Buffer. Bound radioactivity was determined by liquid scintillation spectrophotom-

etry for ^{35}S after overnight extraction of the filters in scintillation fluid optiphase HISAFE 3 (Perkin Elmer, Waltham, USA). Concentrations of radioactive compound were calculated based on the half life of ^{35}S (87.4 days). Experiments were randomised to compensate for position effects in the filter apparatus or unequal sample processing times. Data processing and analysis were blinded for different H_2O_2 concentrations with the help of a colleague.

Data Analysis

Experimental designs were randomised to compensate for the position effects on plates or filter apparatus and unequal sample processing time. Sample sizes were calculated using the G*Power 3.1.2 program with $\alpha < 0.05$, a power of 80% and a defined effect size (derived from pilot experiments). Analysis of concentration-response relationship was performed with simple linear regression using the GraphPad Prism 9 program (GraphPad, San Diego, USA) where y = [^{35}S]-GTPγS bound and x = [H_2O_2]. A P value ≤ 0.05 was considered statistically significant. Normal distribution of the data was assessed using the Kolmogorov-Smirnov test. Data are represented as means $\pm$ standard error of the mean (SEM).

All codes and data are available at https://github.com/user3849/MOR.

Acknowledgements

This research was partially funded by the Deutsche Forschungsgemeinschaft (DFG, German Research Foundation) under Germany's Excellence Strategy – The Berlin Mathematics Research Center MATH+ (EXC-2046/1 project ID: 390685689) and by DFG-STE 477/19-1.

References

Abraham MJ, Murtola T, Schulz R, Páll S, Smith JC, Hess B, Lindahl E. GROMACS: High performance molecular simulations through multi-level parallelism from laptops to supercomputers. SoftwareX. 2015; 1-2:19–25. http://www.sciencedirect.com/science/article/pii/S2352711015000059, doi: 10.1016/j.softx.2015.06.001.

Bhave G, Gereau RW. Posttranslational mechanisms of peripheral sensitization. Journal of Neurobiology. 2004; 61:88–106. doi: 10.1002/neu.20083.

Böhm HJ. The development of a simple empirical scoring function to estimate the binding constant for a protein-ligand complex of known three-dimensional structure. Journal of Computer-Aided Molecular Design. 1994; 8(3):243–256. https://doi.org/10.1007/BF00126743, doi: 10.1007/BF00126743.

Bowen WD, Pert CB. Conformational malleability of opiate receptors: sulfhydryl modification alters ion-induced mu/delta-ligand selectivity shifts in rat striatal sections. Cellular and Molecular Neurobiology. 1982; 2:115–128. doi: https://doi.org/10.1007/BF00711077.

Brandt W, Golbraikh A, Täger M, Lendeckel U. A molecular mechanism for the cleavage of a disulfide bond as the primary function of agonist binding to G-protein-coupled receptors based on theoretical calculations supported by experiments. European Journal of Biochemistry. 1999; 261(1):89–97. doi: 10.1046/j.1432-1327.1999.00224.x.

Bridge L, Mead J, Frattini E, Winfield I, Ladds G. Modelling and simulation of biased agonism dynamics at a G protein-coupled receptor. Journal of theoretical biology. 2018; 442:44–65.

Congreve M, de Graaf C, Swain NA, Tate CG. Impact of GPCR structures on drug discovery. Cell. 2020; 181(1):81–91. doi: 10.1016/j.cell.2020.03.003261.

wwPDB consortium. Protein Data Bank: the single global archive for 3D macromolecular structure data. Nucleic Acids Research. 2019; 47(D1):D520–D528. https://doi.org/10.1093/nar/gky949, doi: 10.1093/nar/gky949.

Essmann U, Perera L, Berkowitz ML, Darden T, Lee H, Pedersen LG. A smooth particle mesh Ewald method. The Journal of Chemical Physics. 1995; 103(19):8577–8593. https://aip.scitation.org/doi/abs/10.1063/1.470117, doi: 10.1063/1.470117.

Gasteiger J, Marsili M. A new model for calculating atomic charges in molecules. Tetrahedron Letters. 1978; 19(34):3181–3184. http://www.sciencedirect.com/science/article/pii/S0040403901949779, doi: 10.1016/S0040-4039(01)94977-9.

Gillespie DT. Exact stochastic simulation of coupled chemical reactions. The journal of physical chemistry. 1977; 81(25):2340–2361.

Gillespie DT. A rigorous derivation of the chemical master equation. Physica A: Statistical Mechanics and its Applications. 1992; 188(1-3):404–425.

Hess B, Bekker H, Berendsen HJC, Fraaije JGEM. LINCS: A linear constraint solver for molecular simulations. Journal of Computational Chemistry. 1997; 18(12):1463–1472. https://onlinelibrary.wiley.com/doi/abs/10.1002/%28SICI%291096-987X%28199709%2918%3A12%3C1463%3A%3AAID-JCC4%3E3.0.CO%3B2-H, doi: 10.1002/(sici)1096-987x(199709)18:12<1463::Aid-jcc4>3.0.Co;2-h.

Hoover WG. Canonical dynamics: Equilibrium phase-space distributions. Physical Review A. 1985; 31(3):1695–1697. https://link.aps.org/doi/10.1103/PhysRevA.31.1695, doi: 10.1103/PhysRevA.31.1695.

Huang J, Rauscher S, Nawrocki G, Ran T, Feig M, de Groot BL, Grubmüller H, MacKerell AD. CHARMM36m: an improved force field for folded and intrinsically disordered proteins. Nature Methods. 2017; 14(1):71–73. https://doi.org/10.1038/nmeth.4067, doi: 10.1038/nmeth.4067.

Humphrey W, Dalke A, Schulten K. VMD: visual molecular dynamics. Journal of Molecular Graphics. 1996; 14(1):33–38. https://www.sciencedirect.com/science/article/pii/0263785596000185, doi: 10.1016/0263-7855(96)00018-5.

Isberg V, de Graaf C, Bortolato A, Cherezov V, Katritch V, Marshall FH, Mordalski S, Pin JP, Stevens RC, Vriend G, Gloriam DE. Generic GPCR residue numbers – aligning topology maps while minding the gaps. Trends in Pharmacological Sciences. 2015; 36(1):22–31. https://doi.org/10.1016/j.tips.2014.11.001, doi: 10.1016/j.tips.2014.11.001.

Jimenez-Vargas NN, Yu Y, Jensen DD, Bok DD, Wisdom M, Latorre R, Lopez C, Jaramillo-Polanco JO, Degro C, Guzman-Rodriguez M, Tsang Q, Snow Z, Schmidt BL, Reed DE, Lomax AE, Margolis KG, Stein C, Bunnett NW, Vanner SJ. Agonist that activates the μ-opioid receptor in acidified microenvironments inhibits colitis pain without side effects. Gut. 2021; Epub ahead of print. doi: 10.1136/gutjnl-2021-324070.

Jorgensen WL, Chandrasekhar J, Madura JD, Impey RW, Klein ML. Comparison of simple potential functions for simulating liquid water. The Journal of Chemical Physics. 1983; 79(2):926–935. https://doi.org/10.1063/1.445869, doi: 10.1063/1.445869.

Kim S, Lee J, Jo S, Brooks Iii CL, Lee HS, Im W. CHARMM-GUI ligand reader and modeler for CHARMM force field generation of small molecules. Journal of Computational Chemistry. 2017; 38(21):1879–1886. https://doi.org/10.1002/jcc.24829, doi: 10.1002/jcc.24829.

Klauda JB, Venable RM, Freites JA, O'Connor JW, Tobias DJ, Mondragon-Ramirez C, Vorobyov I, MacKerell AD, Pastor RW. Update of the CHARMM All-Atom Additive Force Field for Lipids: Validation on Six Lipid Types. The Journal of Physical Chemistry B. 2010; 114(23):7830–7843. https://doi.org/10.1021/jp101759q, doi: 10.1021/jp101759q.

Koehl A, Hu H, Maeda S, Zhang Y, Qu Q, Paggi JM, Latorraca NR, Hilger D, Dawson R, Matile H, Schertler GFX, Granier S, Weis WI, Dror RO, Manglik A, Skiniotis G, Kobilka BK. Structure of the μ-opioid receptor–Gi protein complex. Nature. 2018; 558(7711):547–552. https://doi.org/10.1038/s41586-018-0219-7, doi: 10.1038/s41586-018-0219-7.

Lee J, Patel DS, Ståhle J, Park SJ, Kern NR, Kim S, Lee J, Cheng X, Valvano MA, Holst O, Knirel YA, Qi Y, Jo S, Klauda JB, Widmalm G, Im W. CHARMM-GUI Membrane Builder for Complex Biological Membrane Simulations with Glycolipids and Lipoglycans. Journal of Chemical Theory and Computation. 2019; 15(1):775–786. https://doi.org/10.1021/acs.jctc.8b01066, doi: 10.1021/acs.jctc.8b01066.

Ludwig MG, Vanek M, Guerini D, Gasser JA, Jones CE, Junker U, Hofstetter H, Wolf RM, Seuwen K. Proton-sensing G-protein-coupled receptors. Nature. 2003; 425(6953):93–98. doi: 10.1038/nature01905.

Massaly N, Temp J, Machelska H, Stein C. Uncovering the analgesic effects of a pH-dependent mu-opioid receptor agonist using a model of non-evoked ongoing pain. Pain. 2020; 161:2798–804. doi: 10.1097/j.pain.0000000000001968.

Morris GM, Goodsell DS, Halliday RS, Huey R, Hart WE, Belew RK, Olson AJ. Automated docking using a Lamarckian genetic algorithm and an empirical binding free energy function. Journal of Computational Chemistry. 1998; 19(14):1639–1662. https://onlinelibrary.wiley.com/doi/abs/10.1002/%28SICI%291096-987X%2819981115%2919%3A14%3C1639%3A%3AAID-JCC10%3E3.0.CO%3B2-B, doi: 10.1002/(sici)1096-987x(19981115)19:14<1639::Aid-jcc10>3.0.Co;2-b.

598 **Morris GM**, Huey R, Lindstrom W, Sanner MF, Belew RK, Goodsell DS, Olson AJ. AutoDock4 and AutoDock-
599 Tools4: Automated docking with selective receptor flexibility. Journal of Computational Chemistry. 2009;
600 30(16):2785–2791. https://onlinelibrary.wiley.com/doi/abs/10.1002/jcc.21256, doi: 10.1002/jcc.21256.

601 **Nockemann D**, Rouault M, Labuz D, Hublitz P, McKnelly K, Reis F, Stein C, Heppenstall P. The K+ channel GIRK2
602 is both necessary and sufficient for peripheral opioid-mediated analgesia. EMBO Molecular Medicine. 2013;
603 5:1263–1277. doi: 10.1002/emmm.201201980.

604 **Nosé S**. A molecular dynamics method for simulations in the canonical ensemble. Molecular Physics. 1984;
605 52(2):255–268. https://doi.org/10.1080/00268978400101201, doi: 10.1080/00268978400101201.

606 **Parrinello M**, Rahman A. Polymorphic transitions in single crystals: A new molecular dynamics method. Jour-
607 nal of Applied Physics. 1981; 52(12):7182–7190. https://aip.scitation.org/doi/abs/10.1063/1.328693, doi:
608 10.1063/1.328693.

609 **Proft J**, Weiss N. G Protein Regulation of Neuronal Calcium Channels: Back to the Future. Mol Pharmacol. 2015;
610 87:890–906. doi: 10.1124/mol.114.096008.

611 **Ray S**, Sunkara V, Schütte C, Weber M. How to calculate pH-dependent binding rates for receptor-ligand systems
612 based on thermodynamic simulations with different binding motifs. Molecular Simulation. 2020; 46(18):1443
613 – 1452. doi: 10.1080/08927022.2020.1839660.

614 **Rodriguez-Gaztelumendi A**, Spahn V, Labuz D, Machelska H, Stein C. Analgesic effects of a novel pH-dependent
615 mu-opioid receptor agonist in models of neuropathic and abdominal pain. Pain. 2018; 159:2277–84. doi:
616 10.1097/j.pain.0000000000001328.

617 **Shaw WM**, Yamauchi H, Mead J, Gowers GOF, Bell DJ, Öling D, Larsson N, Wigglesworth M, Ladds G, Ellis T.
618 Engineering a model cell for rational tuning of GPCR signaling. Cell. 2019; 177(3):782–796.

619 **Shea LD**, Neubig RR, Linderman JJ. Timing is everything The role of kinetics in G protein activation. Life Sciences.
620 2000; 68:647–658.

621 **Soteras Gutiérrez I**, Lin FY, Vanommeslaeghe K, Lemkul JA, Armacost KA, Brooks CL, MacKerell AD. Parametriza-
622 tion of halogen bonds in the CHARMM general force field: Improved treatment of ligand–protein interactions.
623 Bioorganic & Medicinal Chemistry. 2016; 24(20):4812–4825. http://www.sciencedirect.com/science/article/pii/
624 S0968089616304576, doi: 10.1016/j.bmc.2016.06.034.

625 **Spahn V**, Del-Vecchio G, Labuz D, Rodriguez-Gaztelumendi A, Massaly N, Temp J, Durmaz V, Sabri P, Reidelbach
626 M, Machelska H, Weber M, Stein C. A nontoxic pain killer designed by modeling of pathological receptor
627 conformations. Science. 2017; 355:966–969.

628 **Stein C**. New concepts in opioid analgesia. Expert opinion on investigational drugs. 2018; 27(10):765–775. doi:
629 10.1080/13543784.2018.1516204.

630 **Walwyn W**, Evans C, Hales T. Beta-arrestin2 and c-Src regulate the constitutive activity and recycling of mu
631 opioid receptors in dorsal root ganglion neurons. Journal of Neuroscience. 2007; 27(19):5092–5104. doi:
632 10.1523/JNEUROSCI.1157-07.2007.

633 **Weis WI**, Kobilka BK. The Molecular Basis of G Protein–Coupled Receptor Activation. Annu Rev Biochem. 2018;
634 87:897–919. doi: 10.1146/annurev-biochem- 060614-033910.

635 **Wheatley M**, Wootten D, Conner M, Simms J, Kendrick R, Logan R, Poyner D, Barwell J. Lifting the lid on GPCRs:
636 the role of extracellular loops. British Journal of Pharmacology. 2012; 165(6):1688–1703. doi: 10.1111/j.1476-
637 5381.2011.01629.x.

638 **Williams JT**, Ingram SL, Henderson G, Chavkin C, von Zastrow M, Schulz S, Koch T, Evans CJ, Christie MJ. Regu-
639 lation of m-Opioid Receptors: Desensitization, Phosphorylation, Internalization, and Tolerance. Pharmaco-
640 logical Reviews. 2013; 65:223–254. doi: 10.1124/pr.112.005942.

641 **Williams M**. The Merck Index: An Encyclopedia of Chemicals, Drugs, and Biologicals, 15th Edition Edited by
642 M.J. O'Neil , Royal Society of Chemistry, Cambridge, UK ISBN 9781849736701; 2708 pages. April 2013, $150
643 with 1-year free access to The Merck Index Online. Drug Development Research. 2013; 74(5):339–339. https:
644 //onlinelibrary.wiley.com/doi/abs/10.1002/ddr.21085, doi: 10.1002/ddr.21085.

645 **Winkelmann S**, Schütte C. Stochastic Dynamics in Computational Biology. Springer; 2020.

Zamponi GW, Snutch TP. Decay of prepulse facilitation of N type calcium channels during G protein inhibition is consistent with binding of a single $\beta\gamma$ subunit. Proc Natl Acad Sci USA. 1998; 95:4035–4039.

Zamponi GW, Striessnig J, Koschak A, Dolphin AC. The Physiology, Pathology, and Pharmacology of Voltage-Gated Calcium Channels and Their Future Therapeutic Potential. Pharmacological Reviews. 2015; 67:821–870. doi: 10.1124/pr.114.009654.

Zhang H, Kenaan C, Hamdane D, Hoa GHB, Hollenberg PF. Effect of Conformational Dynamics on Substrate Recognition and Specificity as Probed by the Introduction of a de Novo Disulfide Bond into Cytochrome P450 2B1. Journal of Biological Chemistry. 2009; 284(38):25678–25686. https://www.sciencedirect.com/science/article/pii/S0021925818810420, doi: 10.1074/jbc.M109.032748.

Zhang P, Johnson P, Zöllner C, Wang W, Wang Z, Montes A, Seidleck B, Blaschak C, Surratt C. Mutation of human mu opioid receptor extracellular "disulfide cysteine" residues alters ligand binding but does not prevent receptor targeting to the cell plasma membrane. Molecular Brain Research. 1999; 72(2):195–204. doi: 10.1016/s0169-328x(99)00241-7.

Zöllner C, Shaqura M, Bopaiah C, Mousa S, Stein C, Schäfer M. Painful inflammation-induced increase in mu-opioid receptor binding and G-protein coupling in primary afferent neurons. Molecular Pharmacology. 2003; 64(2):202–210. doi: 10.1124/mol.64.2.202.

Appendix 1

Nonlinear relationship between binding rates and bound receptors

We showed that the receptor-ligand binding rate k_1 can be affected by a change in its environment (pH value or additional DSB). To understand if these changes in k_1 are linearly or non-linearly influencing the overall activation, we studied the probability of no receptor-ligand binding within the time interval $I = [0, 200]$, where we found the maximum calcium channel inhibition in Fig. 3a. Studying the probability $\text{Prob}(\boldsymbol{RL}(200) = 0)$ of no ligand-bound receptors at time $t = 200$, we found that there was a nonlinear relationship between k_1 and the probability $\text{Prob}(\boldsymbol{RL}(200) = 0)$ (see Fig. 1a). We saw that there is an elbow point $k_1^* \approx 0.0005$ such that the probability of no receptor-ligand complexes increases sharply for $k_1 \leq k_1^*$. We then integrated the probability of no receptor-ligand binding over the interval $[0, 200]$ and found that the elbow point seen earlier had been smoothed (see Fig. 1b). Here we could also see that the relationship between k_1 and the probability of no receptor-ligand binding to be non-linear. We conclude that linear changes in the rate k_1 have a nonlinear effect on their downstream signalling.

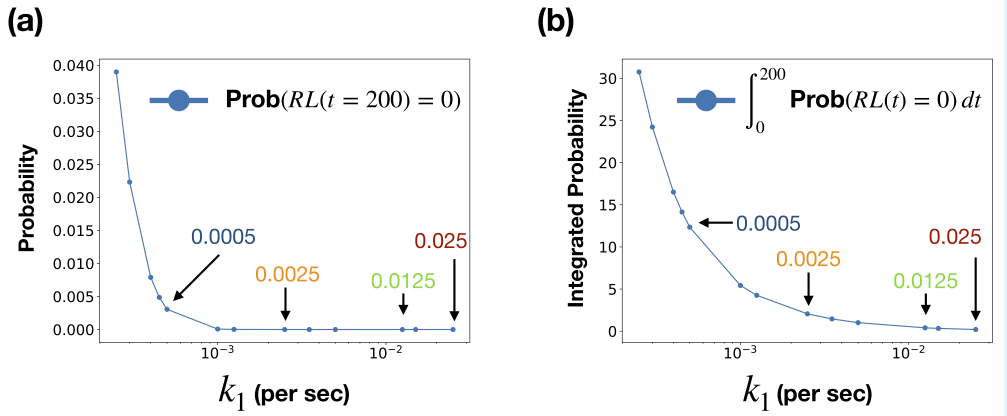

Appendix 1 Figure 1. Probability of no receptor-ligand binding as a function of k_1. (a) Probability of no receptors being bound by ligands at time $t = 200$ for varying k_1 binding rates. (b) Integrated probability of no receptors binding to ligands in the time interval $[0, 200]$ for varying k_1 binding rates. The corresponding position on the x-axis of the k_1 values presented in Table 1 are indicated with arrows.